A Supplementary material

The figures for the unbinned fit are examples for the sample with magnet polarity down and data taken before the July technical stop. The plots are Fig. 4 for the $m(hh)$ ($h = K, \pi$) projection, Fig. 5 for the Δm projection, Figs. 6, 7 for the $\ln(\chi^2_{\rm IP})$ projections, Figs. 8, 9 for the decay-time projection, and Fig. 10 for the first turning point position. Details on the meaning of these variables can be found in LHCb-PAPER-2011-032.

Some of these projections exhibit rather large pull values. It should be noted, however that the relative agreement is rather good throughout. These deviations from ideal behaviour are understood to be intrinsic to the fit method and are well reproduced in simulated pseudo-experiments. The final result, which is related to the difference in lifetime measured in D^0 and $\overline{D}^0$ decays, shows practically no sensitivity to these inaccuracies and any potential effect is covered by the assigned systematic uncertainties.

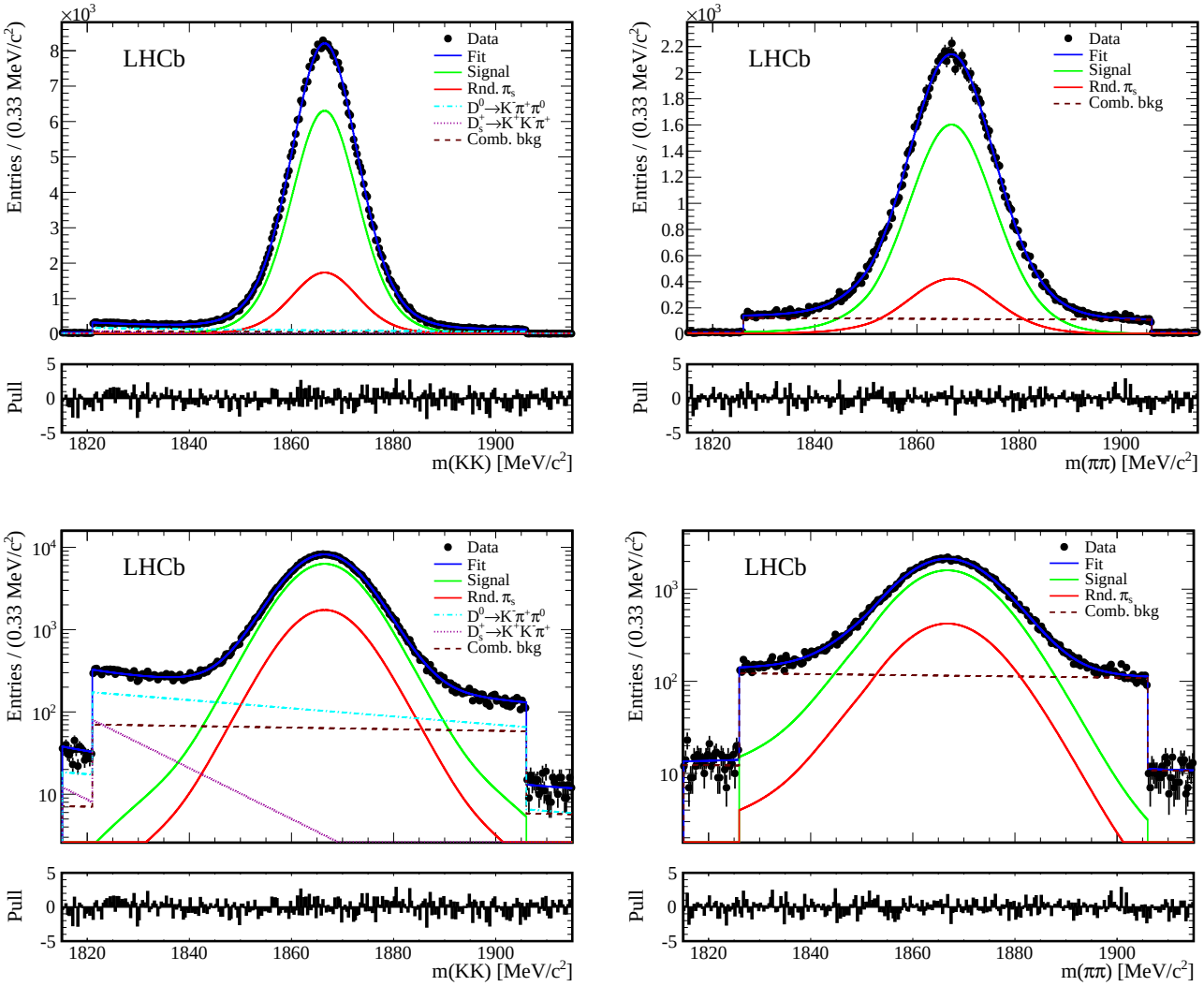

Figure 4: Fits of $m(hh)$ for the (left) $\overline{D}^0 \to K^-K^+$ and (right) $\overline{D}^0 \to \pi^-\pi^+$ candidates with magnet polarity down for the earlier run period with (top) linear scale and (bottom) semi-log scale.

The plots for the binned fit method show examples of D^0 decays for three different decay time bins for data taken with magnet polarity down. The $m(hh)$ projection is shown in Figs. 12, 13, the Δm projection is shown in

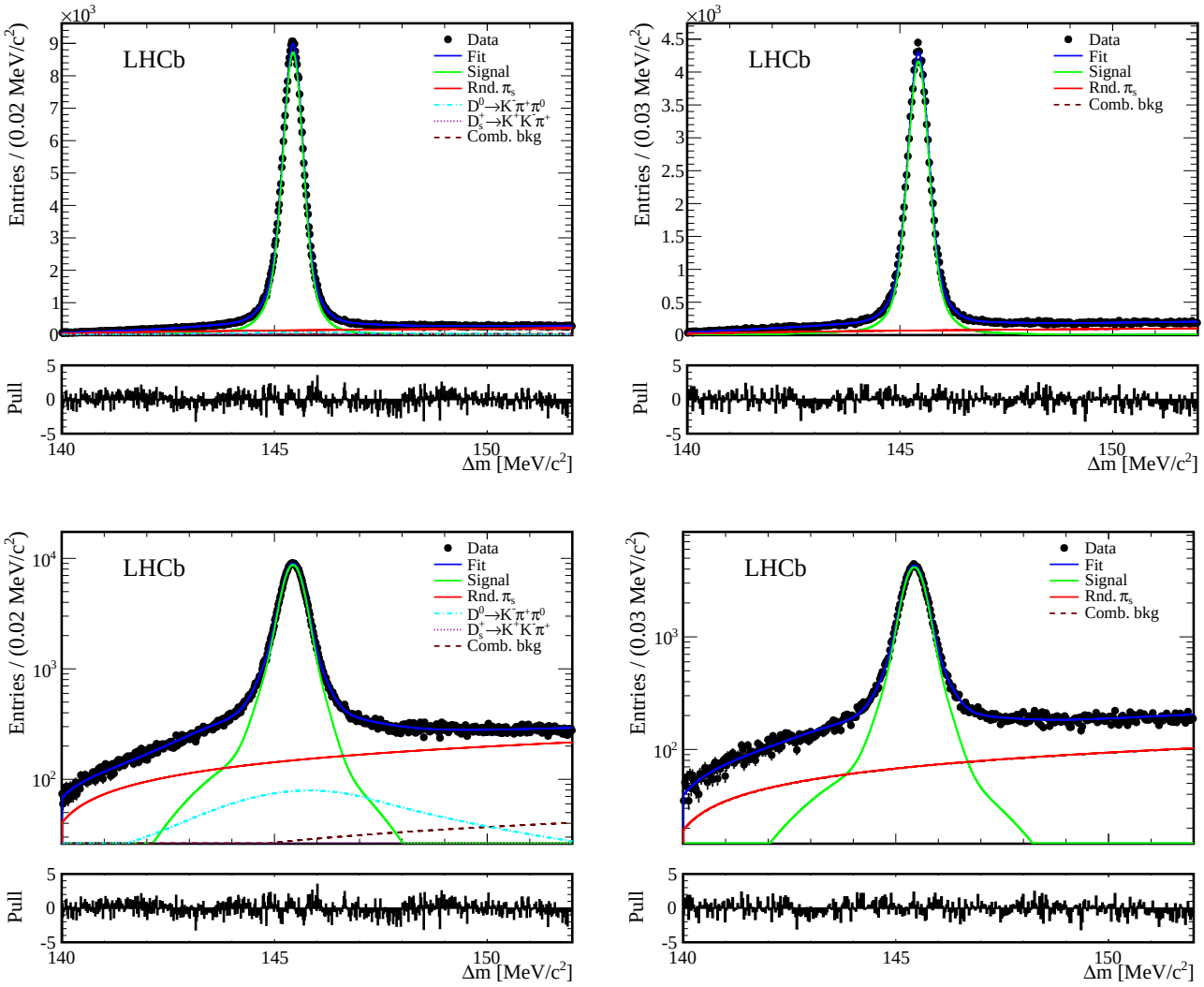

Figure 5: Fits of Δm for the (left) $\overline{D}^0 \to K^-K^+$ and (right) $\overline{D}^0 \to \pi^-\pi^+$ candidates with magnet polarity down for the earlier run period with (top) linear scale and (bottom) semi-log scale.

Figs. 14, 15, and the $\ln(\chi^2_{\rm IP})$ projection is shown in Fig. 16, 17. Finally, Fig. 18 shows $R(t)$ for the two final states.

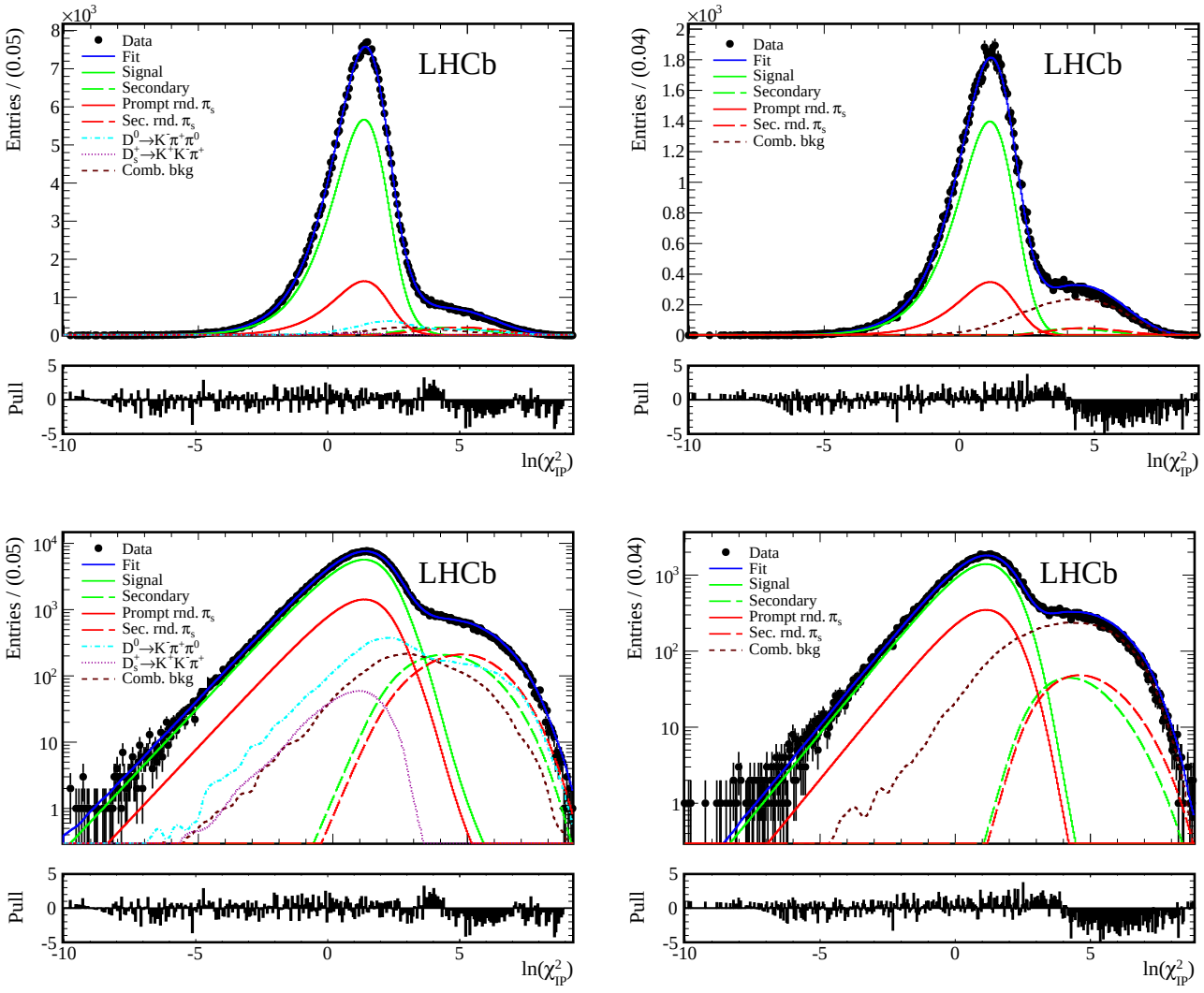

Figure 6: Fits of $\ln(\chi^2_{\rm IP})$ for the (left) $D^0 \to K^-K^+$ and (right) $D^0 \to \pi^-\pi^+$ candidates with magnet polarity down for the earlier run period with (top) linear scale and (bottom) semi-log scale.

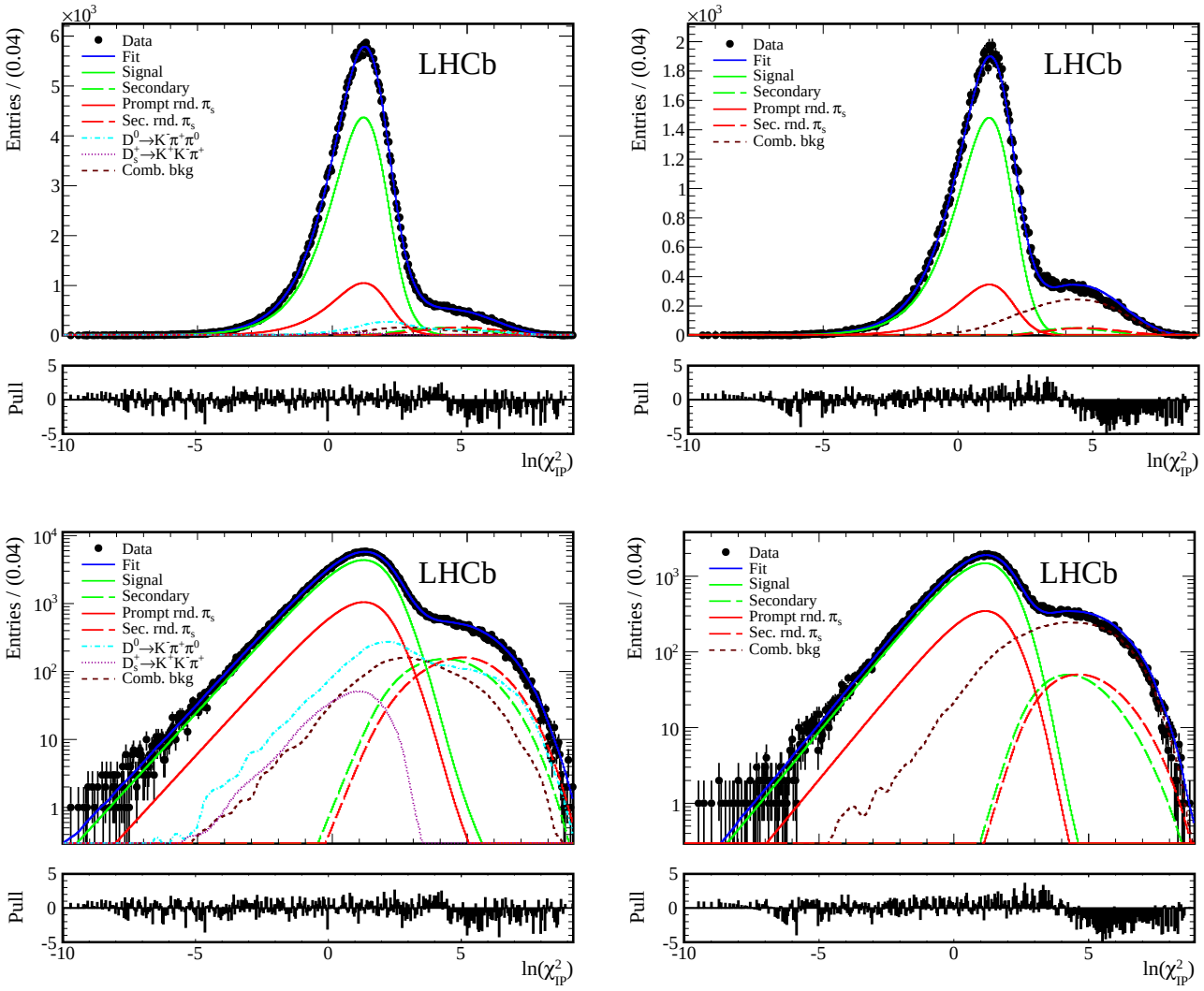

Figure 7: Fits of $\ln(\chi^2_{\rm IP})$ for the (left) $\overline{D}^0 \to K^-K^+$ and (right) $\overline{D}^0 \to \pi^-\pi^+$ candidates with magnet polarity down for the earlier run period with (top) linear scale and (bottom) semi-log scale.

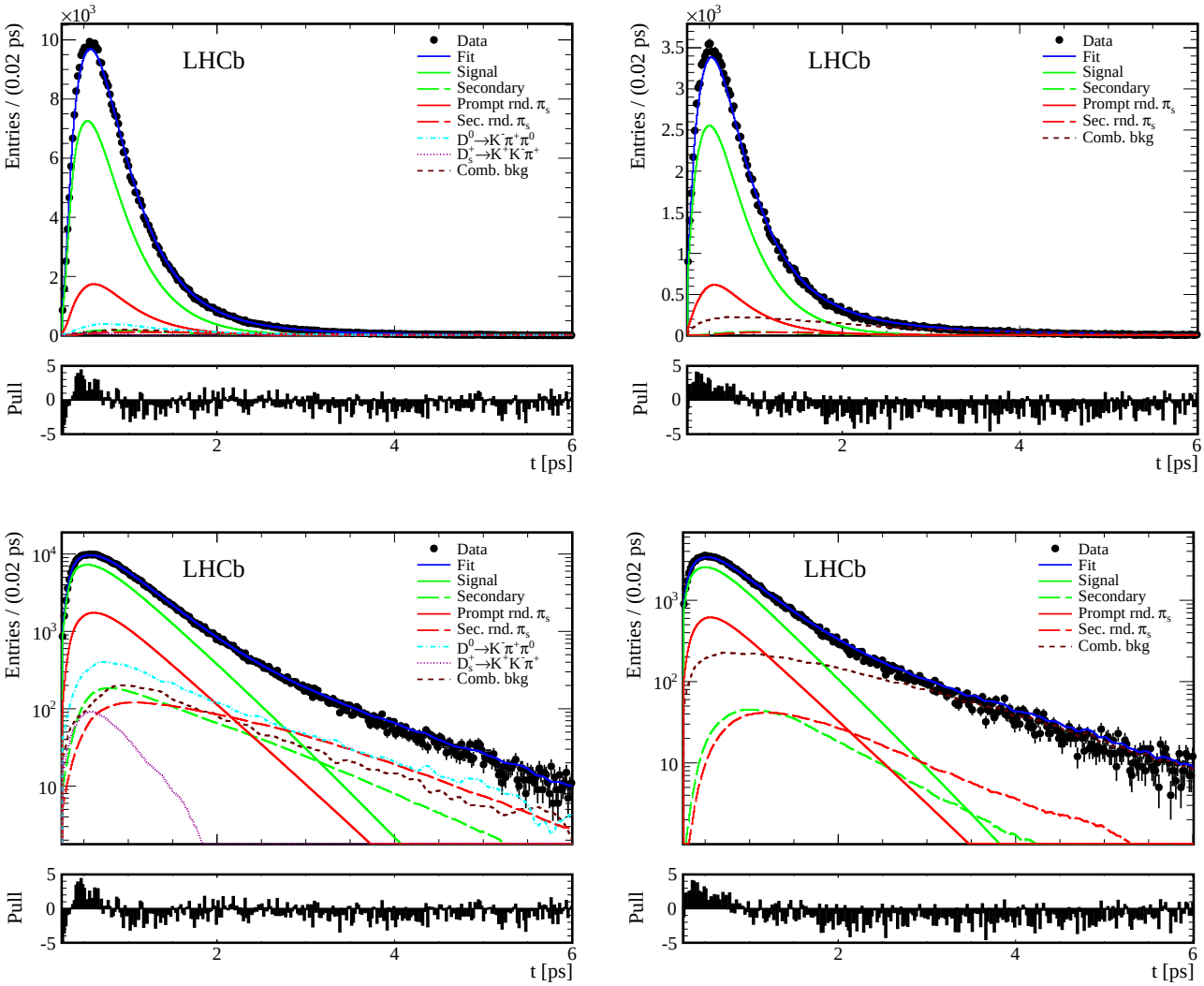

Figure 8: Fits of decay time for the (left) $D^0 \to K^-K^+$ and (right) $D^0 \to \pi^-\pi^+$ candidates with magnet polarity down for the earlier run period with (top) linear scale and (bottom) semi-log scale.

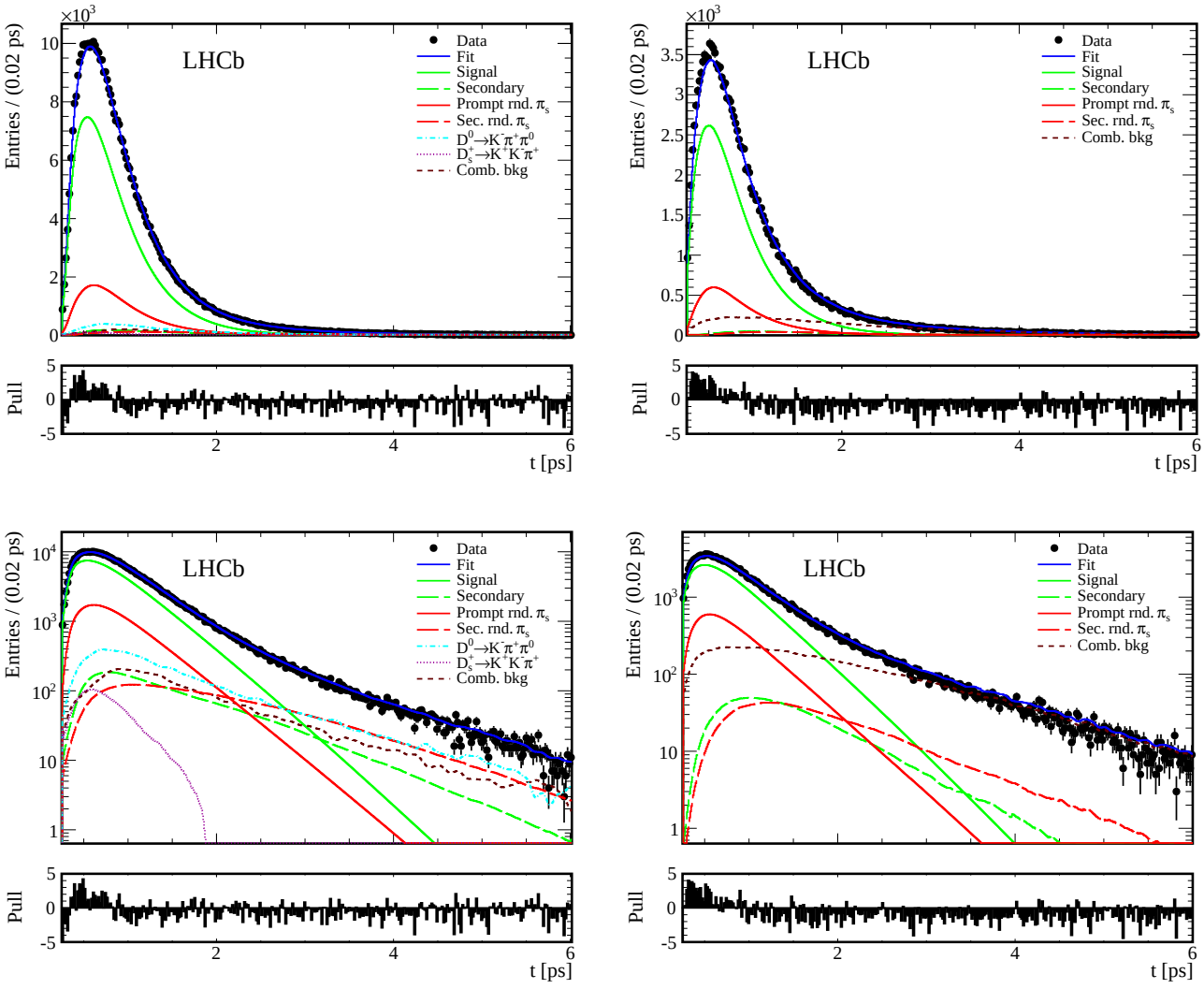

Figure 9: Fits of decay time for the (left) $\overline{D}^0 \to K^-K^+$ and (right) $\overline{D}^0 \to \pi^-\pi^+$ candidates with magnet polarity down for the earlier run period with (top) linear scale and (bottom) semi-log scale.

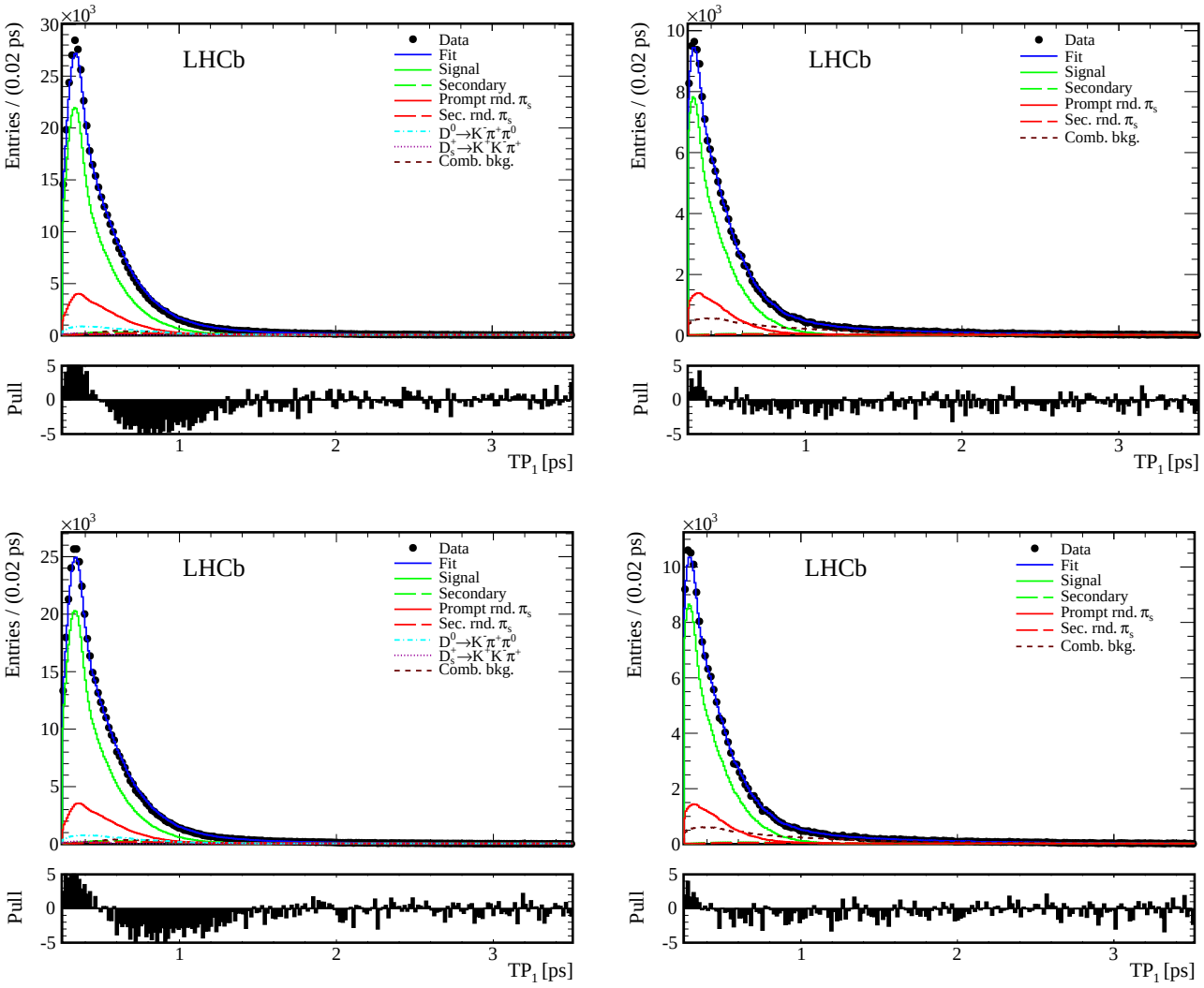

Figure 10: Projection of first turning point position (see LHCb-PAPER-2011-032) for the final states (left) K^-K^+ and (right) $\pi^-\pi^+$ with magnet polarity down for the earlier run period for (top) D^0 and (bottom) $\overline{D}^0$ decays. As described in the text, the large pulls in these plots do not affect the fit result.

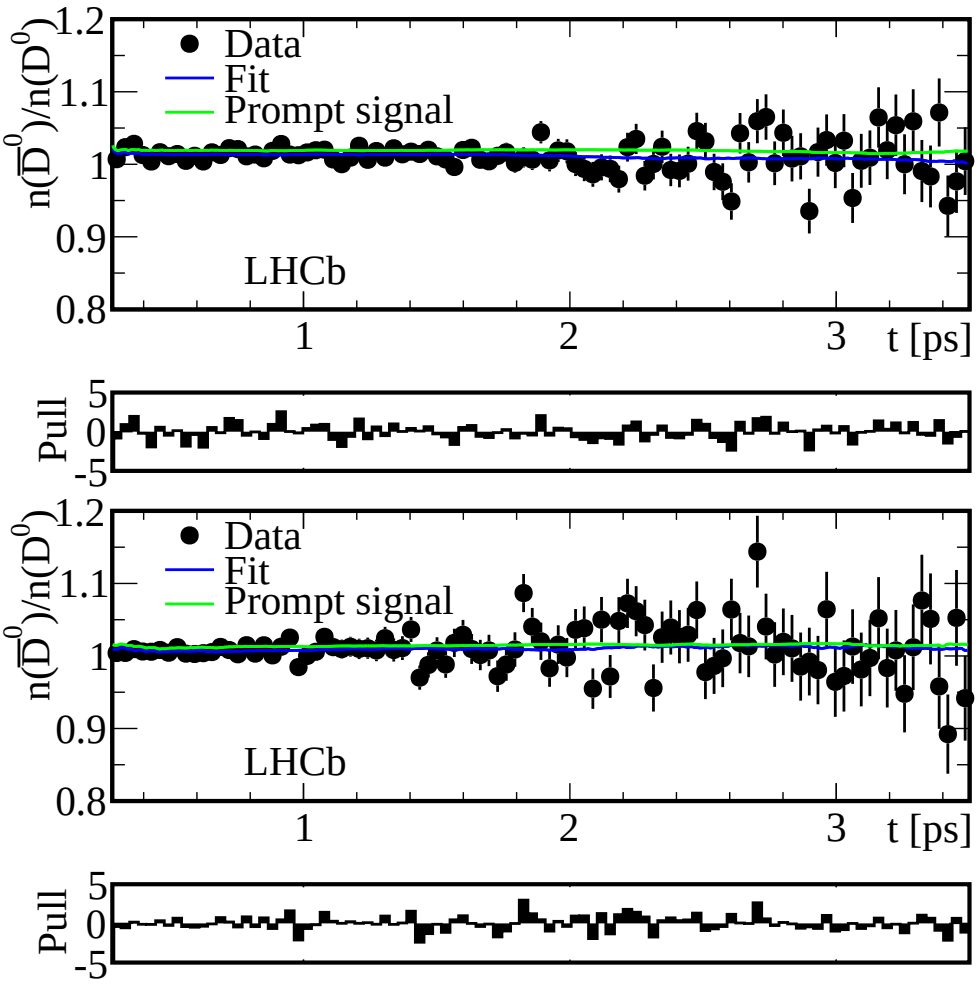

Figure 11: Ratio of $\overline{D}^0$ to D^0 for (top) K^-K^+ and (bottom) $\pi^-\pi^+$. Shown are the ratios for data, the full fit distribution, and the prompt signal component. The plots are based on the full data set.

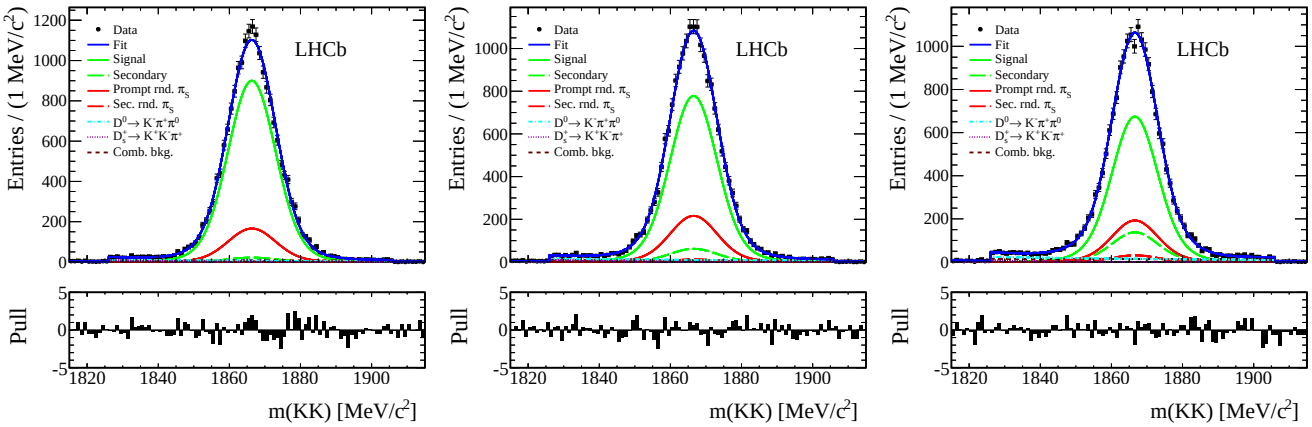

Figure 12: Fits of $m(hh)$ for $D^0 \to K^-K^+$ decays for decay time bins (left to right) $0.25 - 0.37$ ps, $0.74 - 0.78$ ps, and $1.55 - 1.80$ ps.

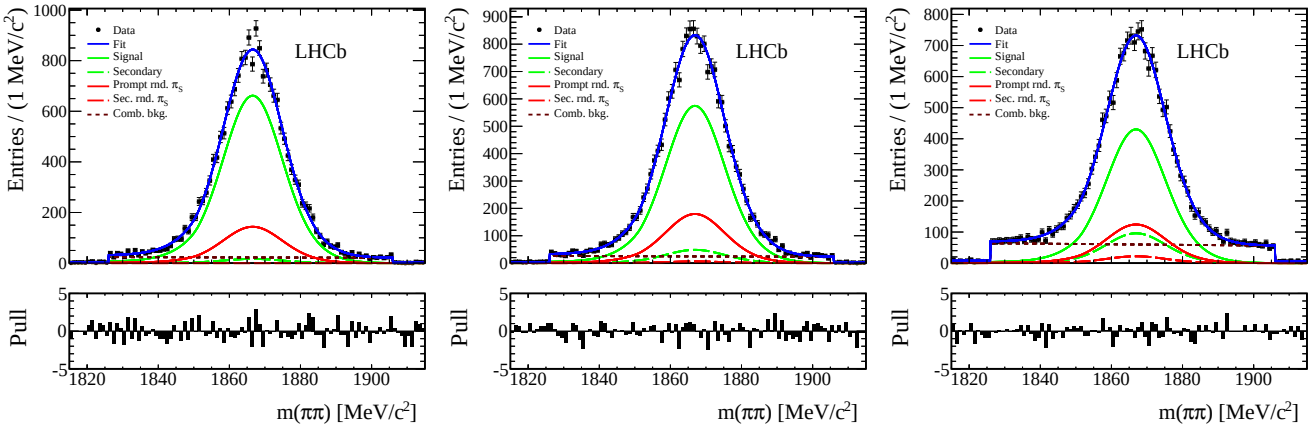

Figure 13: Fits of $m(hh)$ for $D^0 \to \pi^-\pi^+$ decays for decay time bins (left to right) $0.25 - 0.41$ ps, $0.72 - 0.86$ ps, and $1.29 - 1.82$ ps.

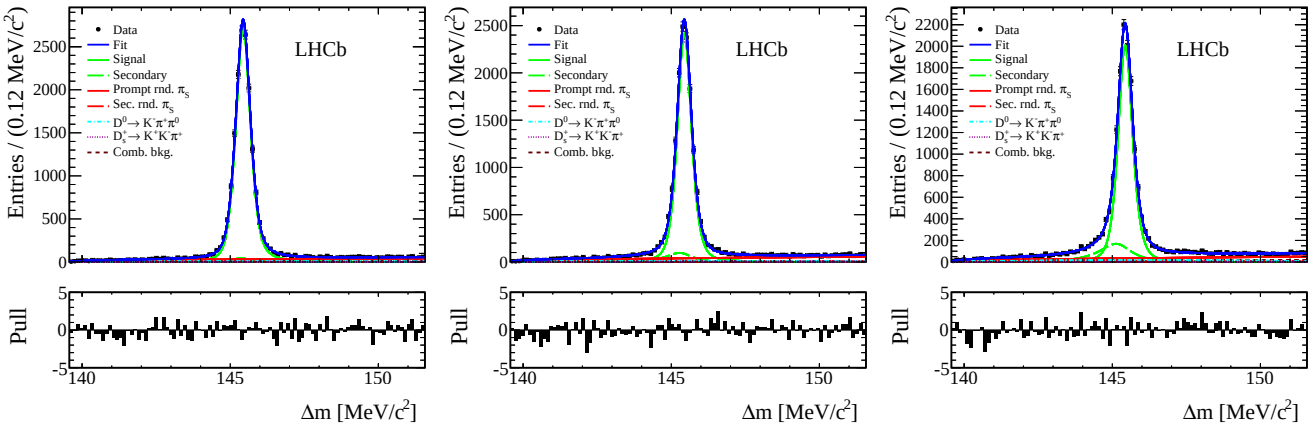

Figure 14: Fits of Δm for $D^0 \to K^-K^+$ decays for decay time bins (left to right) $0.25 - 0.37\,\text{ps}$, $0.74 - 0.78\,\text{ps}$, and $1.55 - 1.80\,\text{ps}$.

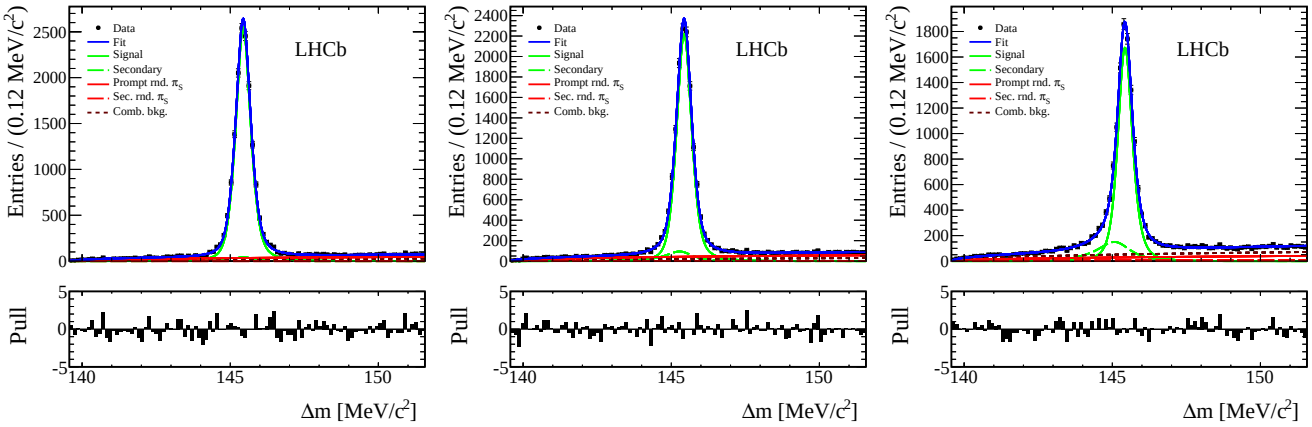

Figure 15: Fits of Δm for $D^0 \to \pi^-\pi^+$ decays for decay time bins (left to right) $0.25 - 0.41\,\text{ps}$, $0.72 - 0.86\,\text{ps}$, and $1.29 - 1.82\,\text{ps}$.

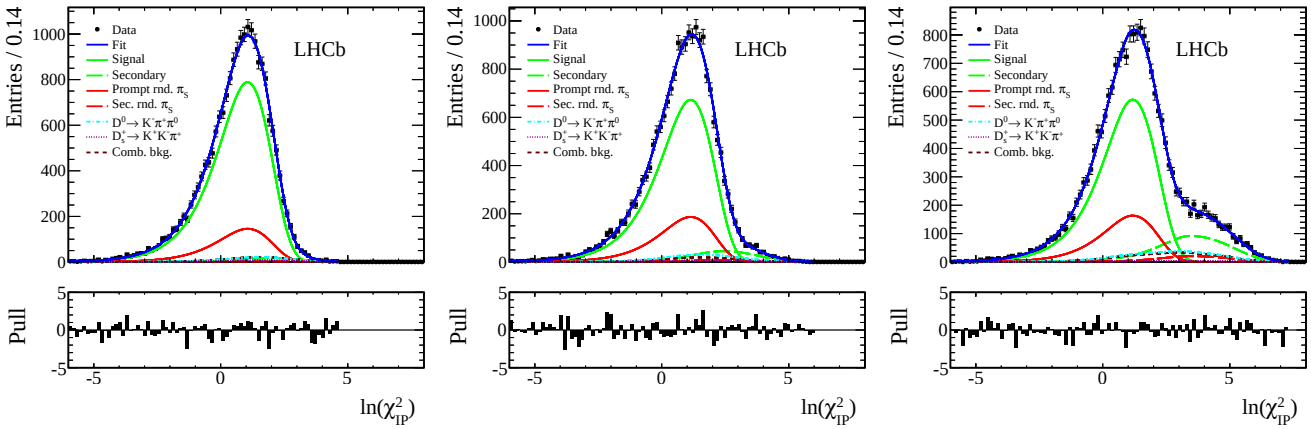

Figure 16: Fits of D^0 $\ln(\chi^2_{\rm IP})$ for $D^0 \to K^-K^+$ decays for decay time bins (left to right) $0.25-0.37\,$ps, $0.74-0.78\,$ps, and $1.55-1.80\,$ps.

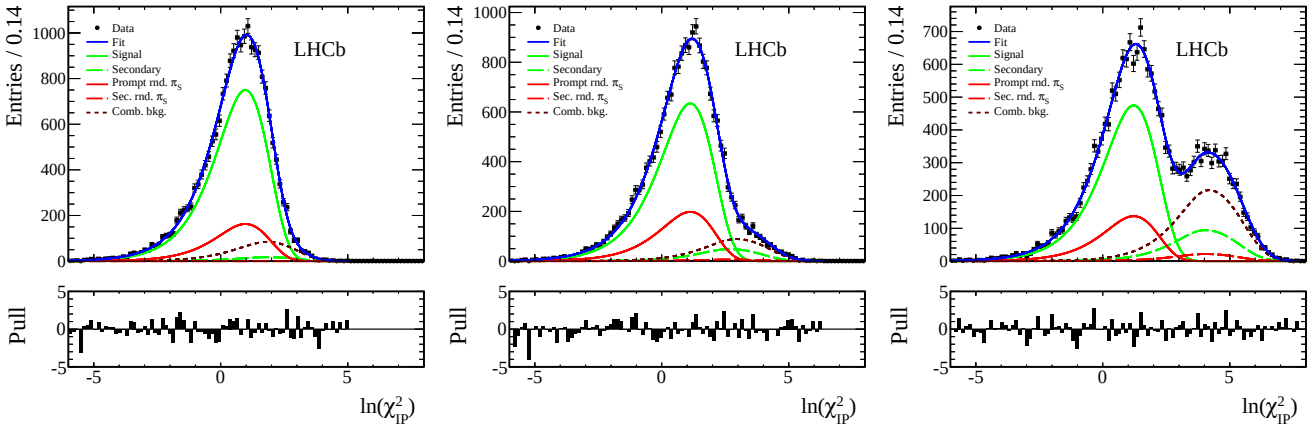

Figure 17: Fits of D^0 $\ln(\chi^2_{\rm IP})$ for $D^0 \to \pi^-\pi^+$ decays for decay time bins (left to right) $0.25-0.41\,$ps, $0.72-0.86\,$ps, and $1.29-1.82\,$ps.

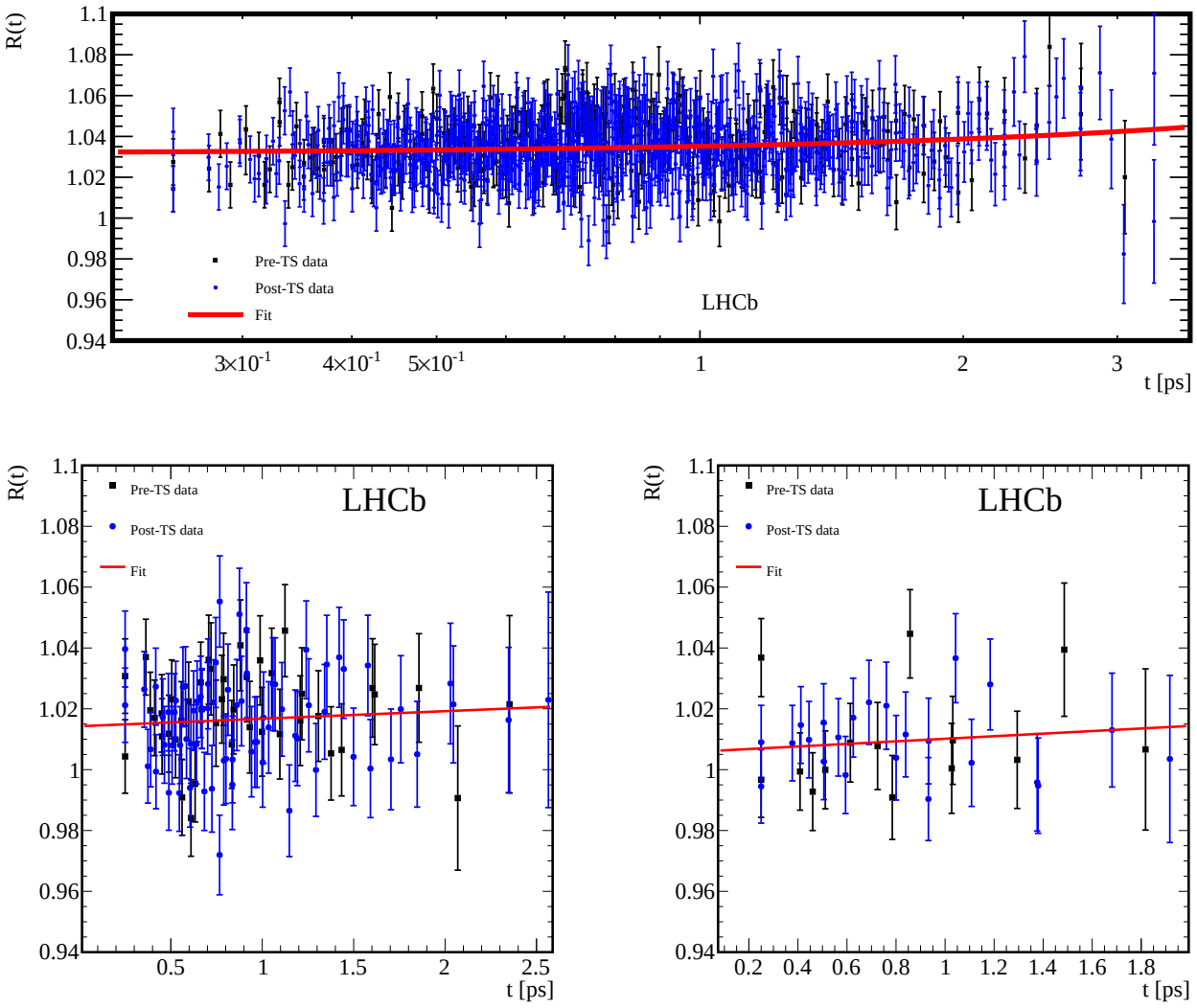

Figure 18: Evolution of the D^0-$\overline{D}^0$ yield ratio with decay time for (top) $D^0 \to K^-\pi^+$ decays, (bottom left) $D^0 \to K^-K^+$ decays and (bottom right) $D^0 \to \pi^-\pi^+$ decays, with the two data-taking periods shown with different symbols. The line shows the linear fit to extract A_Γ.